Metrol. Meas. Syst., Vol. 32 (2025), No. 3
DOI: 10.24425/mms.2025.154681

PAN POLSKA AKADEMIA NAUK

METROLOGY AND MEASUREMENT SYSTEMS
Index 330930, ISSN 0860-8229
www.metrology.wat.edu.pl

M&MS

TESTING POSITIONING SYSTEM FOR GROUND PENETRATING RADAR USING MULTI-DEGREE-OF-FREEDOM INDUSTRIAL ROBOT

Tomasz Kraszewski[1)], Jarosław Panasiuk[2)], Paweł Słowak[1)], Piotr Kaniewski[1)]

1) *Military University of Technology, Faculty of Electronics, Gen. S. Kaliskiego 2, 00-908 Warsaw, Poland* (✉ *piotr.kaniewski@wat.edu.pl*)
2) *Military University of Technology, Faculty of Mechatronics, Armament and Aerospace, Gen. S. Kaliskiego 2, 00-908 Warsaw, Poland*

Abstract

This paper introduces a navigation system, and a data processing algorithm tailored for a handheld ground-penetrating radar (GPR), along with results from real-world tests conducted using a physical model. Handheld GPR systems are indispensable for scanning challenging and inaccessible terrains, particularly in detecting buried landmines and other explosive remnants of war, where vehicle-mounted GPR systems cannot operate effectively. Building on prior research, which focused on a system designed with stationary and mobile ultrawideband radio transceivers tested via simulations, this study addresses practical challenges encountered in a real-world physical model. A novel data processing algorithm is proposed to handle key issues, including a variable number of distance measurements per estimation step and the presence of measurement outliers. Furthermore, the methodology and results of real-world testing of the positioning system, conducted using an industrial robot for controlled experimentation, are presented and discussed.

Keywords: ground-penetrating radar, GPR, extended Kalman filter, EKF, ultrawideband radio, UWB, industrial robot.

1. Introduction

Testing positioning and navigation systems typically includes assessment of their accuracy [1]. This process usually begins with simulations; however, real-world testing of the physical model is crucial to confirm that the system performs as expected under realistic conditions and that its parameters align with the design assumptions. Assessment of the positioning accuracy is typically done by comparing position estimates provided by the system with a synchronized stream of data from another, significantly more accurate system, which is considered a reference system [2]. This reference system should be at least an order of magnitude more accurate than the tested one.

When designing and testing high-accuracy positioning and navigation systems, identifying an appropriate reference system can be challenging or even impossible. This issue also applies to a positioning system for *handheld ground penetrating radar* (HH-GPR) which was designed by the authors at the Faculty of Electronics, Military University of Technology, Warsaw, Poland, as detailed in [3, 4]. The system was developed to realize the positioning of the HH-GPR antenna during terrain scanning, as the accurate determination of the scanning path is important to correctly assemble acquired radargrams and create high-quality GPR images [5]. Our system uses highly accurate distance measurements between stationary and mobile *ultrawideband* (UWB) radio transceivers, achieving positioning errors typically in order of single centimetres. This level of accuracy was confirmed by simulations, and their results are documented in [3, 4, 6].

After developing a physical model of this system, we encountered challenges in determining its errors. Unfortunately, its level of accuracy is comparable to that of the most precise geodetic-

Article history: received December 13, 2024; revised May 26, 2025; accepted July 25, 2025; available online August 25, 2025.

grade receivers of *global navigation satellite systems* (GNSS) using *real-time kinematic* (RTK) corrections [7]. While such receivers are often applied as a reference when testing less accurate systems, our case required an even better-accuracy source of positioning data to serve as a reliable reference.

An alternative to employing a high-accuracy reference system is to constrain the tested system to follow a predefined, time-tagged trajectory and compare its positioning results with this trajectory. This approach is feasible, albeit limited to relatively short trajectories, by utilizing industrial robots constructed as multi-jointed arms and a gripper, capable of executing multi-degree-of-freedom motions [8]. As the HH-GPR antenna motion can be segmented into numerous short sections, this limited range of robot motions does not impose limitations on our testing process.

The requirement for precise and repeatable movements, often resulting from a precisely defined manipulation of a tool or an object taken using a gripper, is one of the main reasons for the popularity of industrial robots. Such robots are characterized by high precision, achieving positional repeatability with an accuracy of up to 0.02 mm (although in the case of robots with a larger lifting capacity it is often reduced to 0.2 mm) with a simultaneous linear speed of up to 4 m/s [8], enabling efficient operation in demanding applications.

The use of robots extends beyond production processes. Industrial robots are also increasingly prevalent in research applications [9]. In this context, the ability to repeat experiments multiple times while maintaining consistent kinematic and dynamic parameters for the robot arm's movement is invaluable. Considering the load capacity of industrial robot manipulators reaching up to one and a half tons, the scope of applications of this type of solution is remarkably broad. Currently, a new trend in the design of industrial robot control systems introduces user-friendly interfaces that allow to input data regarding the configuration of the manipulator as well as its spatial trajectory [10]. These advanced features, as well as availability of industrial robots at the Faculty of Mechatronics, Armament and Aerospace, Military University of Technology, have enabled the authors to advance the development of the positioning system for HH-GPR and assess the accuracy of its physical model in realistic scenarios.

Designing and testing of the physical model of the UWB-based positioning system revealed practical issues that needed to be addressed and had not been previously considered in the design presented in our paper [3]. These issues included variable number of UWB distance measurements observed in each step of data processing, which was solved by using *sequential extended Kalman filter* (SEKF) instead of the previously applied *extended Kalman filter* (EKF). Moreover, measurement outliers, occasionally observed in UWB distance measurements due to the propagation issues were eliminated from the processed data stream by applying statistical tests on innovations [11] implemented in the processing algorithm.

The main contributions of this paper include the development of a navigation data processing algorithm for estimating HH-GPR antenna position and other parameters of its motion, using sequential measurements processing and elimination of the measurement outliers via statistical tests on innovations. Additionally, the paper presents a methodology and detailed results of real-world tests of the UWB-based positioning system, conducted using an industrial robot.

This paper is organized as follows. Section 2 describes the positioning system, its state-space model and the data processing algorithms implemented in it. The methodology of tests and their results are presented in Section 3 and Section 4 contains the discussion.

2. Materials and methods

The subsequent section of the paper presents a concise overview of the UWB-based positioning system for handheld ground penetrating radar (HH-GPR) and its associated

mathematical model. This brief description is included here to ensure the completeness of the paper and to facilitate understanding of its further parts. For an in-depth explanation of the system, its methods of application and potential uses readers are referred to [3] and [4]. Subsection 2.3 introduces novel data processing algorithms designed by the authors to address the UWB sensors limitations and propagation issues encountered in the physical model of our positioning system.

2.1. Positioning system

The positioning system depicted in Fig. 1 is composed of four stationary UWB modules $M_1 \div M_4$ with known locations, referred to as UWB beacons, and two mobile UWB modules: M_A mounted on the GPR antenna and M_S attached to the shoulder of the radar operator (sapper). Distance measurements between the mobile and the stationary modules $d_{A1} \div d_{A4}$ and $d_{S1} \div d_{S4}$ are processed within the positioning system to estimate the HH-GPR antenna position as it moves along the scanning path.

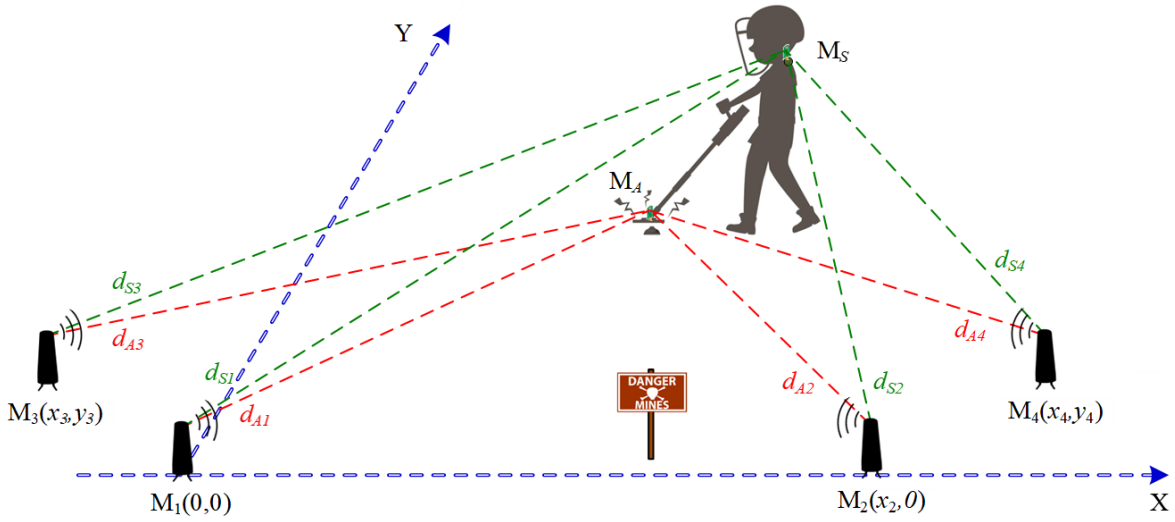

Fig. 1. Components and measurements in UWB-based positioning system.

The proposed system utilizes a local horizontal reference frame, established ad hoc when the beacons are deployed around the scanned region. It is assumed that the M_1 module is positioned at the origin $(0,0)$ and the M_2 module lies along the OX axis. The unknown coordinates x_2, x_3, y_3, x_4, y_4 are calculated through an autocalibration procedure [6, 12], which is performed prior to the system executing its primary task of positioning. The autocalibration process involves analysing distance measurements between the beacons and iteratively solving a set of non-linear equations that relate those measurements and the coordinates of the stationary modules.

2.2. Mathematical models

In positioning applications, model-based algorithms are commonly employed to process incoming streams of measurements. The algorithms rely on underlying models that include a dynamics model, which describes the temporal changes of the modeled variables and enables the prediction of their future values, as well as an observation model which defines the relationship between these variables and the measurements.

The dynamics model, depending on the system, can be linear or non-linear and can be expressed as a vector differential equation (continuous model) or a vector difference equation (discrete model). In [3] we proposed the use of two linear dynamics models commonly applied in motion tracking – such as in robotics [13, 14] and radar applications [15, 16] – namely, nearly-*constant-velocity* (CV) model and nearly-*constant-acceleration* (CA) model, along with a novel non-linear model based on the *pendulum equation* (PND). Simulation results presented in [3] and [4] indicate that the CV and CA models provide similar accuracy in our application. Therefore, in this work, we employ only the simpler CV model and the more advanced PND model, which achieves superior positioning accuracy.

The CV model is given by the following linear differential equation:

$$\text{CV:}\quad \begin{bmatrix} \dot{x}_A \\ \dot{v}_x \\ \dot{y}_A \\ \dot{v}_y \end{bmatrix} = \begin{bmatrix} 0 & 1 & 0 & 0 \\ 0 & 0 & 0 & 0 \\ 0 & 0 & 0 & 1 \\ 0 & 0 & 0 & 0 \end{bmatrix} \begin{bmatrix} x_A \\ v_x \\ y_A \\ v_y \end{bmatrix} + \begin{bmatrix} 0 & 0 \\ 1 & 0 \\ 0 & 0 \\ 0 & 1 \end{bmatrix} \begin{bmatrix} u_{v_x} \\ u_{v_y} \end{bmatrix} \tag{1}$$

and the PND model by the following non-linear differential equation:

$$\text{PND:}\quad \begin{bmatrix} \dot{x}_A \\ \dot{y}_A \\ \dot{x}_S \\ \dot{y}_S \\ \dot{\theta} \\ \dot{\omega} \\ \dot{a} \end{bmatrix} = \begin{bmatrix} \omega(y_A - y_S) \\ -\omega(x_A - x_S) \\ 0 \\ 0 \\ \omega \\ -\frac{a}{l} sin\,\theta \\ 0 \end{bmatrix} + \begin{bmatrix} 0 & 0 & 0 \\ 0 & 0 & 0 \\ 1 & 0 & 0 \\ 0 & 1 & 0 \\ 0 & 0 & 0 \\ 0 & 0 & 0 \\ 0 & 0 & 1 \end{bmatrix} \begin{bmatrix} u_{x_S} \\ u_{y_S} \\ u_a \end{bmatrix}, \tag{2}$$

where:

- x_A, y_A – coordinates of the M_A module position,
- x_S, y_S – coordinates of the M_S module position,
- u_{x_S}, u_{y_S} – Gaussian white noises modeling random M_S module motions,
- l – length of the HH-GPR handle (horizontal distance between M_S and M_A),
- θ – angle between the horizontal projection of the HH-GPR antenna handle and the central axis of the scanning section,
- ω – angular velocity of the M_A module motion,
- a – acceleration forcing the M_A module motion,
- u_a – Gaussian white noise representing random changes of a.

As shown, the CV dynamics model is linear and takes the following standard form [15]:

$$\dot{\mathbf{x}}(t) = \mathbf{F}(t)\mathbf{x}(t) + \mathbf{G}(t)\mathbf{u}(t) \tag{3}$$

which was converted to its discrete counterpart [15] before using it in the processing algorithm:

$$\mathbf{x}(k+1) = \mathbf{\Phi}(k+1, k)\mathbf{x}(k) + \mathbf{w}(k), \tag{4}$$

where:

- $\mathbf{x}$ – state vector,
- $\mathbf{u}$ – vector of continuous disturbances,
- $\mathbf{F}$ – fundamental matrix,
- $\mathbf{G}$ – matrix of disturbances,
- $\mathbf{w}$ – vector of discrete disturbances,
- $\mathbf{\Phi}$ – transition matrix.

In the sampling of the CV continuous model, we obtained two matrices required in the data processing algorithm using this model, namely, the transition matrix $\mathbf{\Phi}(k+1,k)$ and the covariance matrix of discrete disturbances $\mathbf{Q}(k) = \mathrm{E}[\mathbf{w}(k)\mathbf{w}(k)^{\mathrm{T}}]$, and their final forms can be found in [4].

The PND model, differently than CV, is non-linear and has the following standard form [15]:

$$\dot{\mathbf{x}}(t) = \mathbf{f}[\mathbf{x}(t)] + \mathbf{G}(t)\mathbf{u}(t) \tag{5}$$

which was used directly in its continuous form within the data processing algorithm to predict new values of the state vector. Sampling of this model was also required, but it needed to be performed at each step of the algorithm. The method of sampling the PND model and the formulas for the resulting matrices are detailed in [3].

The observation model for the system and algorithm using the PND dynamics model is represented by the following discrete equations [3, 4]:

$$\begin{bmatrix} d_{A1}(k) \\ d_{A2}(k) \\ d_{A3}(k) \\ d_{A4}(k) \\ d_{S1}(k) \\ d_{S2}(k) \\ d_{S3}(k) \\ d_{S4}(k) \end{bmatrix} = \begin{bmatrix} \sqrt{(x_A(k)-x_1)^2+(y_A(k)-y_1)^2} \\ \sqrt{(x_A(k)-x_2)^2+(y_A(k)-y_2)^2} \\ \sqrt{(x_A(k)-x_3)^2+(y_A(k)-y_3)^2} \\ \sqrt{(x_A(k)-x_4)^2+(y_A(k)-y_4)^2} \\ \sqrt{(x_S(k)-x_1)^2+(y_S(k)-y_1)^2+h^2} \\ \sqrt{(x_S(k)-x_2)^2+(y_S(k)-y_2)^2+h^2} \\ \sqrt{(x_S(k)-x_3)^2+(y_S(k)-y_3)^2+h^2} \\ \sqrt{(x_S(k)-x_4)^2+(y_S(k)-y_4)^2+h^2} \end{bmatrix} + \begin{bmatrix} v_{A1}(k) \\ v_{A2}(k) \\ v_{A3}(k) \\ v_{A4}(k) \\ v_{S1}(k) \\ v_{S2}(k) \\ v_{S3}(k) \\ v_{S4}(k) \end{bmatrix}, \tag{6}$$

where:

d_{Aj} – distance between a j-th beacon and the M_A module,
d_{Sj} – distance between a j-th beacon and the M_S module,
x_j, y_j – coordinates of a j-th beacon position,
x_A, y_A – coordinates of the M_A module position,
x_S, y_S – coordinates of the M_S module position,
h – sapper's arm height,
v_{Aj}, v_{Sj} – distance measuring errors for M_A and M_S modules.

When the CV dynamics model is employed in the data processing algorithm, the estimated position variables are limited to the coordinates of the $\mathrm{M_A}$ module's position, and the observation model includes only the four distance measurements $d_{\mathrm{A1}} \div d_{\mathrm{A4}}$. Both observation models are non-linear and have the following standard form [15]:

$$\mathbf{z}(k) = \mathbf{h}[\mathbf{x}(k)] + \mathbf{v}(k), \tag{7}$$

where:

$\mathbf{z}$ – measurement vector,
$\mathbf{v}$ – vector of measurement errors,
$\mathbf{h}(\cdot)$ – non-linear observation vector function.

To implement the data processing algorithm, it was also necessary to define the covariance matrix of measurement errors, $\mathbf{R}(k) = \mathrm{E}[\mathbf{v}(k)\mathbf{v}(k)^{\mathrm{T}}]$. Its final form is provided in [3] and [4].

2.3. Algorithms of estimation

The navigation data processing algorithms employed in our system are based on the equations of the EKF [1, 15, 17] and are illustrated in Fig. 2 and Fig. 3. The algorithm depicted in Fig. 2 utilizes the linear CV dynamics model, while the algorithm in Fig. 3 employs the non-linear PND dynamics model. Both algorithms rely on distinct, yet non-linear observation models, which are described by the (6) for the PND model or only its upper part composed of the first four equations for the CV model.

Each EKF begins with a one-time initialization and then enters a loop in which alternately executes prediction and correction steps. The EKF requires linearization of non-linear dynamics and/or observation models. For the filter utilizing the linear CV dynamics model, only the observation model requires linearization, which is performed during the calculation of the observation matrix $\mathbf{H}(k)$. In contrast, for the filter based on the non-linear PND dynamics model, both the dynamics and observation models must be linearized, with the dynamics model linearization carried out during the computation of the fundamental matrix $\mathbf{F}(t)$.

In both EKFs we introduced modifications to enable sequential processing of incoming measurements. Within the correction step of both filters, an internal loop replaces the standard correction step [3] with a series of corrections, where each available measurement is processed individually. The internal loop employs its own indexing variable i which increments after each processed measurement. At the start of the loop (for $i = 0$), the correction results are initialized using the prediction results:

$$\hat{\mathbf{x}}_{k|k,0} = \hat{\mathbf{x}}_{k|k-1}, \tag{8}$$

$$\mathbf{P}_{k|k,0} = \mathbf{P}_{k|k-1}. \tag{9}$$

The correction process, which involves calculating improved estimates $\hat{\mathbf{x}}_{k|k,i}$ and their covariance matrices of filtration errors $\mathbf{P}_{k|k,i}$ continues for successive incremented values of i until the last available measurement numbered m has been processed. The number of measurements can be different in every step k and the filter does not require a fixed size of the measurement vector $\mathbf{z}$. This way we addressed the problem of a variable number of distance measurements observed in the UWB-based positioning system at different steps k.

In the real system, a pair of UWB modules may occasionally fail to complete their radio transaction, resulting in missing distance measurement. Consequently, the measurement vector $\mathbf{z}(k)$ contains a varying number of measurements at each step k. The modified algorithm, referred to in this paper as the sequential extended Kalman filter (SEKF), effectively handles this issue.

Another practical issue observed in the UWB-based positioning system is the occurrence of measurement outliers in the distance measurements between various pairs of UWB modules. These outliers may arise due to propagation challenges, such as multipath errors, which occur particularly when the shortest signal path is obstructed by an obstacle and only reflected signals traveling along longer paths are received. If not properly addressed, these elevated distance measurement errors could result in significant increases in positioning errors.

In both presented algorithms we addressed the mentioned problem by implementing a solution for detecting outliers in the measurements and eliminating them from the processed data. The removal of outliers is based on the results of statistical tests on the innovations [11]. For each individual distance measurement $\mathbf{z}_{k,i}$ a residual, *i.e.* a difference between the actual and the predicted measurement is calculated:

$$\mathbf{e}_{k,i} = \mathbf{z}_{k,i} - \mathbf{h}\left(\hat{\mathbf{x}}_{k|k,i-1}\right). \tag{10}$$

It represents a realization of the innovations process, which is a Gaussian, uncorrelated, zero-mean stochastic process. Since the EKFs also calculate the diagonal elements of the covariance matrix of innovations $\mathbf{R}_{\mathbf{e}_{k,i}}$ which represent theoretical variances of innovations, the statistics ρ_i calculated in the EKFs has χ^2 distribution with one degree of freedom.

Using the cumulative distribution function of the χ^2 distribution, we determined a threshold λ that will rarely be exceeded for typical distance measurements and will easily be exceeded by outliers. We selected $\lambda = 3.84$ corresponding to the commonly assumed level of type I error (false positive) and significance level $\alpha = 0.05$. For this threshold, approximately 5% of valid measurements may be rejected statistically, however the threshold remains low enough to reliably detect outliers. The results of simulations presented further show that removal of such a small part of valid measurements does not compromise accuracy of positioning.

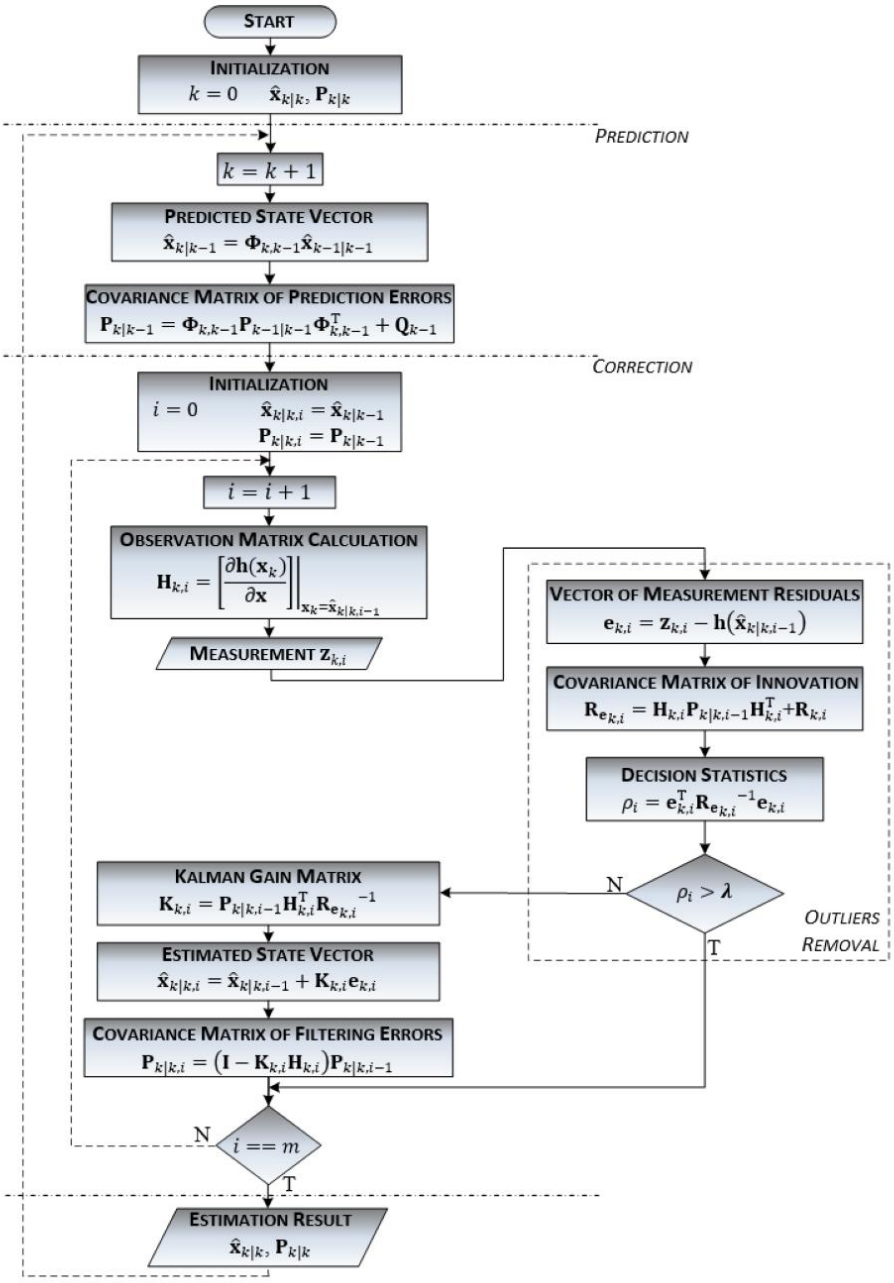

Fig. 2. Block diagram of the EKF algorithm for the linear dynamics model CV and the nonlinear observation model.

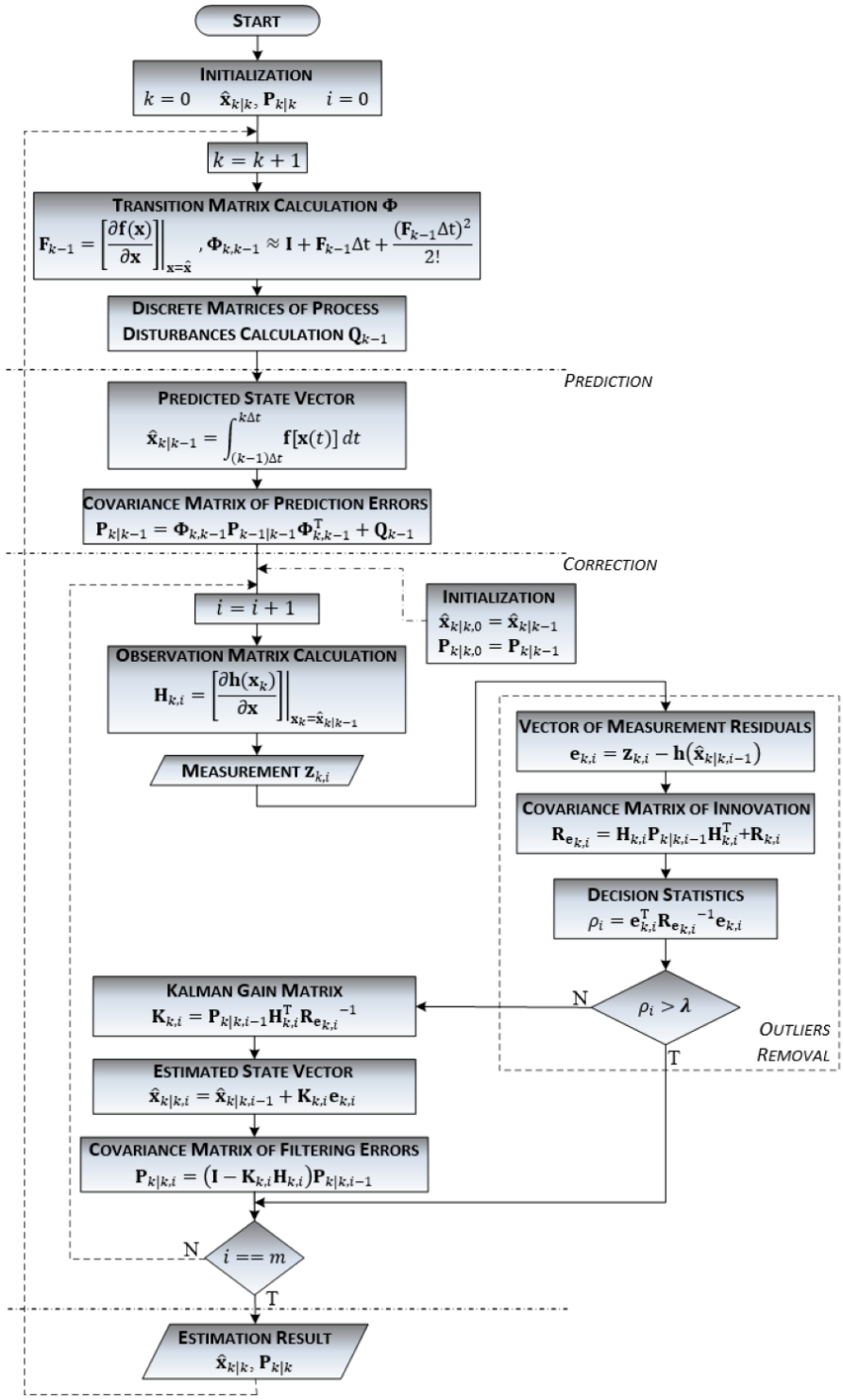

Fig. 3. Block diagram of the EKF algorithm for the nonlinear dynamics model PND and the nonlinear observation model.

3. Experiments and results

3.1. Preparation to experiments

The experimental evaluation of the positioning system's accuracy was conducted in multiple stages and involved extensive preparation. Initially, the UWB beacons $M_1 \div M_4$ were deployed in the laboratory of industrial robots at the Faculty of Mechatronics, Armament and Aerospace,

Military University of Technology. These beacons had been designed and constructed by a team from the Institute of Radioelectronics, Faculty of Electronics, Military University of Technology, including some of the authors of this paper. The beacons contain P440 UWB radio transceivers manufactured by TDSR [18].

Two mobile UWB radio transceivers of the same type were mounted on an industrial robot FANUC R-2000iC/125L. The $\mathrm{M_A}$ module (antenna module) was attached to the gripper at the end of the robot's arm, while the $\mathrm{M_S}$ module (sapper module) was positioned above the robot at a height of $h = 1.65$ m, representing the assumed distance from the ground to the sapper's shoulder. The limited space in the laboratory and existing obstacles between the robot and the $\mathrm{M_1} \div \mathrm{M_4}$ beacons imposed constraints on their possible locations. However, the beacons were arranged to mimic deployment in a typical demining operation, *i.e.* spaced as widely as possible and distributed in front of the scanning area. The stationary UWB modules were mounted on tripods at the same height as the $\mathrm{M_A}$ module to ensure consistency. The UWB beacons deployed in the laboratory and the $\mathrm{M_A}$ module installed in the robot's gripper during the experiment are shown in Fig. 4. One of the beacons and the antenna module are highlighted with red ovals.

Fig. 4. The UWB beacons and the antenna module in the griper of industrial robot during experiments.

The layout of stationary UWB modules during the real-world tests closely resembled their configurations used in the simulations presented in our earlier work [3]. However, due to the limited space of the laboratory, achieving a comparable separation between the modules was not feasible. In the previously presented results in [3], the separation distances were on the order of tens of meters, whereas in the current experiments, these distances were limited to a range of single meters.

To better align the conditions of the simulations with those of the real-world tests, we conducted additional simulations prior to the experiments. These simulations replicated the precise locations of the beacons and mobile modules as deployed in the laboratory. The distances between various UWB modules were measured using a laser rangefinder Bosch PLR 50C with an accuracy of ± 2 mm.

The autocalibration procedure described in the section 2.1 of this paper was applied to calculate the positions of the UWB beacons and the sapper module in a local reference frame and these positions are given in Tab. 1.

Tab. 1. Locations of $M_1 \div M_4$ and M_S modules in the laboratory during experiments.

$\mathbf{M_1}$	$\mathbf{M_2}$	$\mathbf{M_3}$	$\mathbf{M_4}$	$\mathbf{M_S}$
[0, 0]	[3.013, 0]	[4.475, 1.380]	[-1.955, 1.369]	[1.428, 5.371]

The above module locations were utilized to simulate the operation of the positioning system in a configuration consistent with that employed in the real-world experiments. During the simulations, a segment of the HH-GPR scanning trajectory was generated by numerically integrating the differential equations of the PND model and the obtained HH-GPR antenna trajectory was further used as a reference. Subsequently, distance measurements from both mobile modules, M_A and M_S, to all stationary beacons ($M_1 \div M_4$) were generated. Measurement errors were simulated assuming standard deviations of a $\sigma = 0.02$ m consistent with the specification of the P440 modules. The generated distance measurements were processed using the new versions of the algorithms (SEKF) with CV and PND dynamics models, referred to as SEKF-CV and SEKF-PND, respectively.

Next, to evaluate the performance of the algorithms in case of measurement outages, 25 percent of the distance measurements from the previously generated dataset were randomly removed, and this reduced dataset was again processed by the algorithms SEKF-CV and SEKF-PND. The estimated trajectories of the HH-GPR antenna for both filters, without and with the measurement outages are presented in Fig. 5, where SAP denotes the sapper location, and CV and PND indicate trajectories estimated by the SEKF-CV and SEKF-PND algorithms, respectively.

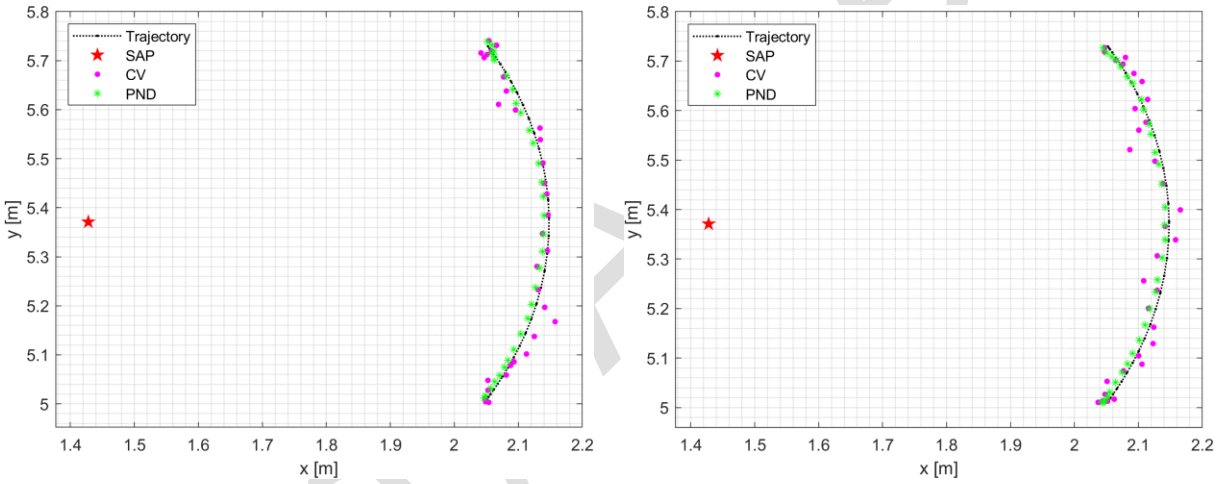

Fig. 5. Estimated trajectory of HH-GPR antenna with SEKF-CV and SEKF-PND filters: without the measurement outages (left panel), and with the measurement outages (right panel).

The simulations confirmed the proper operation of the newly proposed SEKF-CV and SEKF-PND filters. Furthermore, even with the more compact layout of the UWB beacons, their behaviour and accuracy remained consistent, achieving centimetre-level precision, similar to that observed in configurations with more widely spaced stationary UWB modules. As expected, and in accordance with our previous findings in [3], the SEKF-PND algorithm, which utilizes the PND dynamics model, produces more accurate estimates of the antenna position compared to the SEKF-CV algorithm, which employs the simpler CV model.

As can be seen, the sequential algorithms, designed specifically for the situation of temporary outages of distance measurements in the UWB-based positioning system, properly handle the incomplete measurements at various processing steps which confirmed that they can be used for processing real-world datasets. Another conclusion is that even a relatively large number of missed distance measurements in the designed system does not significantly reduce the accuracy of positioning and the errors remain still of the order of single centimeters.

3.2. Experiments and their results

Having confirmed that the proposed SEKF-CV and SEKF-PND filters work properly even for a changeable size of the measurement vectors and having assessed the expected accuracy of the UWB positioning system in its configuration identical to the one deployed in the laboratory of industrial robots, the physical model of the UWB-based positioning system was tested with use of the real-world data.

First, the same trajectory as used in the simulations was programmed into the position registers of the FANUC R-2000iC/125L industrial robot. This required using a programme ROBOGUIDE®, a specialized off-line modelling and simulation environment for testing robotic systems. Programmed trajectory consisted of time stamps and successive positions and orientations of the robot's gripper. ROBOGUIDE® generated and verified the final trajectory, which described the robot's gripper movement to these successive positions. The modeled laboratory setup, with the robot and all the stationary and mobile UWB modules, as well as the visible trajectory of the HH-GPR antenna are presented in Fig. 6, where BS1–BS4 denote the locations of base stations containing the UWB beacons $M_1 \div M_4$.

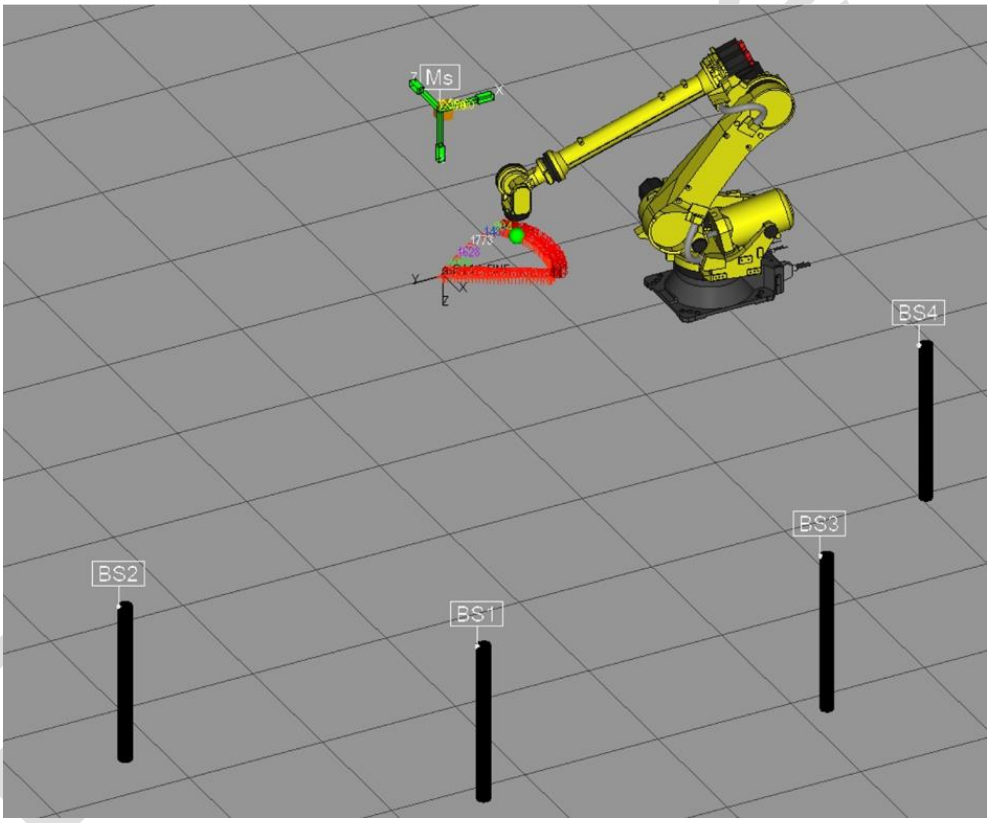

Fig. 6. Model of the laboratory stand for testing UWB-positioning system in ROBOGUIDE®.

The actual experiment involved the use of a real FANUC R-2000iC/125L industrial robot with the HH-GPR antenna mounted in its gripper. The robot's arm followed the above-described predefined trajectory, and during this motion, distance measurements between the mobile modules M_A and M_S and all $M_1 \div M_4$ beacons were acquired. To register these data, the RangeNet® application by TDSR, designed for configuring and communicating with the P440 UWB transceivers was utilized. The acquired distance measurements are presented in Fig. 7.

The uneven spacing between successive measurements for various pairs of UWB modules confirms the presence of outages in the real-world data. Additionally, occasional atypical data

points, significantly deviating from the regular trajectories formed by the measurements for various UWB pairs suggests existence of the measurement outliers.

The recorded dataset of UWB distances was subsequently processed offline using the SEKF-CV and SEKF-PND filters. The trajectory of HH-GPR antenna estimated by both algorithms is shown in Fig. 8. The left panel of the figure presents this trajectory estimated with SEKF-PND filter within the entire layout of the laboratory stand, where triangles indicate the locations of UWB modules $M_1 \div M_4$. The right panel presents an enlarged fragment, showing the position estimates for SEKF-CV and SEKF-PND alongside the reference trajectory.

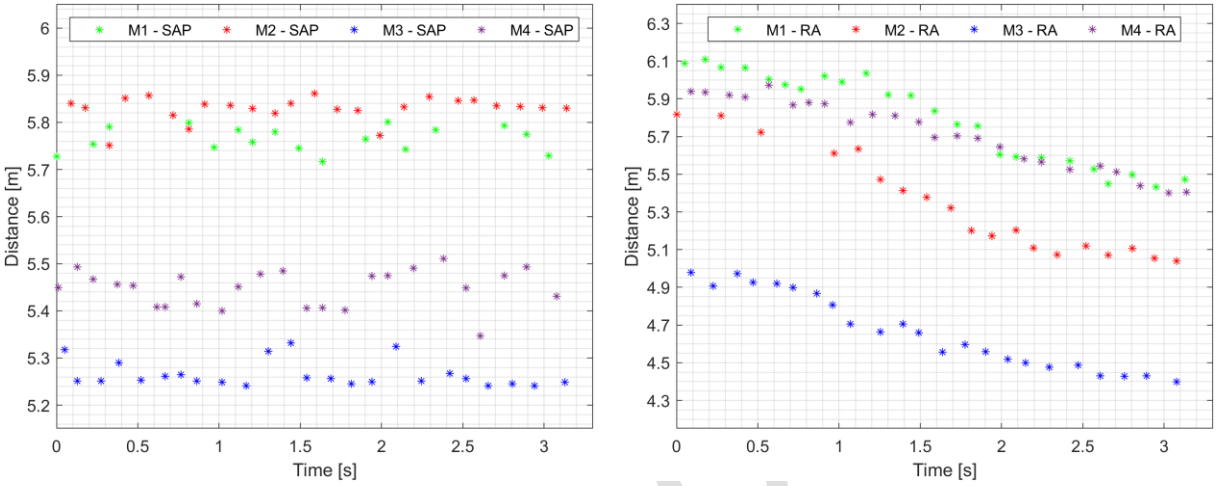

Fig. 7. Distance measurements acquired during the real-world experiment: between the UWB beacons $M_1 \div M_4$ and the sapper (SAP) (left panel), and between the beacons $M_1 \div M_4$ and the radar antenna (RA) (right panel).

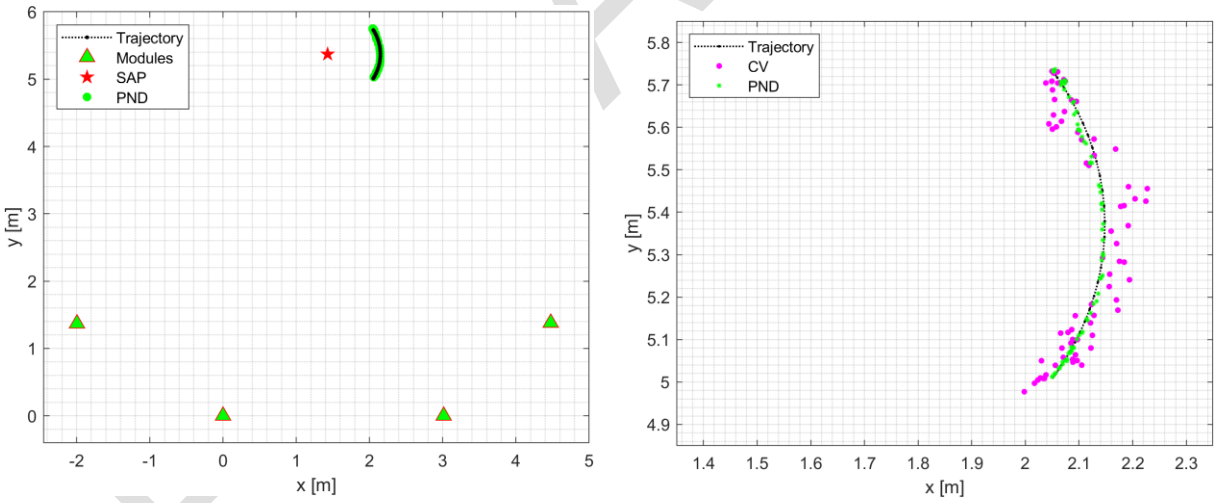

Fig. 8. Trajectory of HH-GPR antenna estimated with SEKF-CV and SEKF-PND filters in the experiment.

As demonstrated, the sequential algorithms, specifically designed to handle temporary outages of distance measurements in the UWB-based positioning system, effectively manage incomplete data at various processing steps. This confirms their suitability for processing real-world datasets. Furthermore, the results indicate that even a relatively large proportion of missed distance measurements in the system and presence of the measurement outliers does not significantly compromise positioning accuracy, with errors remaining on the order of single centimetres.

Comparing the results obtained with two distinct filters SEKF-CV and SEKF-PND one can conclude that the SEKF-PND algorithms occurs significantly more accurate than the

SEKF-CV, and it should be the preferrable solution for HH-GPR antenna positioning unless simplicity of the system and reduced computations are of paramount importance.

4. Conclusions

This paper presents two algorithms, SEKF-CV and SEKF-PND, developed for processing distance measurements in our previously designed and constructed UWB-based positioning system. These algorithms leverage the equations of the EKF and employ two alternative approaches to model the motion of the HH-GPR antenna: the simple CV model and the more sophisticated PND model.

Both algorithms incorporate modifications aimed at addressing challenges commonly associated with the propagation of radio signals, as observed in real-world measurements of distances between UWB transceivers. These challenges include measurement outages and the presence of outliers. To handle outages and the variable size of the measurement vector at different processing steps, the algorithms were redesigned to sequentially process the incoming measurement stream. The issue of outliers was addressed by applying statistical tests on the innovations calculated within the filters and rejecting measurements exhibiting abnormally large errors.

The proposed algorithms were rigorously tested in simulations and validated through controlled experiments using an industrial robot, the FANUC R-2000iC/125L. The robot enabled precise replication of predefined trajectories, providing highly accurate reference data for comparison with the positioning results obtained from the UWB-based system. The experimental results presented in this paper are consistent with the simulation outcomes and confirm that the proposed positioning system achieves centimetre-level accuracy in estimating the HH-GPR antenna trajectory.

In particular, the SEKF-PND algorithm demonstrated superior accuracy, making it a strong candidate for use in the described positioning system. Testing both filters with real-world measurement data further validated the robustness of the proposed algorithms, showing their capability to handle variations in the number of available distance measurements at each estimation step and to effectively mitigate the impact of measurement outliers. These results underscore the reliability and practicality of the designed positioning system for applications requiring precise trajectory estimation.

Acknowledgements

This work was supported by the Military University of Technology, Poland, under research project UGB/22-056/2025/WAT.

References

[1] Grewal, M. S., Weill, L. R., & Andrews, A. P. (2007). *Global positioning systems, inertial navigation, and integration* (2nd ed.). John Wiley & Sons, Inc. https://doi.org/10.1002/0470099720

[2] Kawecki, J., Brewer, J., Cao, J., & Baldwin, J. (2016). Can't deny the truth: Air force upgrades to a better field reference system for testing GPS denial. *GPS World*, *27*, 22–29.

[3] Kaniewski, P., & Kraszewski, T. (2023). Estimation of Handheld Ground-Penetrating Radar Antenna Position with Pendulum-Model-Based Extended Kalman Filter. *Remote Sensing*, *15*(3), 741. https://doi.org/10.3390/rs15030741

[4] Kraszewski, T. (2023). Metoda estymacji położenia anteny ręcznego radaru penetracji gruntu. Wojskowa Akademia Techniczna.

[5] Pasternak, M., & Kaczmarek, P. (2019). Continuous wave ground penetrating radars: state of the art. In *XII Conference on Reconnaissance and Electronic Warfare Systems* (Vol. 11055, p. 10). SPIE. https://doi.org/10.1117/12.2524524

[6] Kaniewski, P., & Kraszewski, T. (2020). Novel Algorithm for position Estimation of Handheld Ground-Penetrating Radar Antenna. In *21st International Radar Symposium (IRS)* (pp. 100–102). https://doi.org/10.23919/irs48640.2020.9253877

[7] Kaplan, E. D., & Hegarty, C. (2017). *Understanding GPS/GNSS: Principles and applications* (3rd ed.). https://trid.trb.org/view/1472240

[8] FANUC Europe Corporation. (2019). *FANUC LR Mate 200iD datasheet*. https://www.fanuc.eu/pl/pl/roboty/robot-strona-filtrowania/lrmate-series

[9] Panasiuk, J., & Kaczmarek, W. (2019). Robotization of production processes. Wydawnictwo Naukowe PWN

[10] Dzedzickis, A., Subačiūtė-Žemaitienė, J., Šutinys, E., Samukaitė-Bubnienė, U., & Bučinskas, V. (2021). Advanced Applications of Industrial Robotics: New trends and possibilities. *Applied Sciences*, *12*(1), 135. https://doi.org/10.3390/app12010135

[11] Jun, S., Szmajda, M., Khoma, V., Khoma, Y., Sabodashko, D., Kochan, O., & Wang, J. (2020). Comparison of methods for correcting outliers in ECG-based biometric identification. *Metrology and Measurement Systems*, 387–398. https://doi.org/10.24425/mms.2020.132784

[12] Kaniewski, P., Kraszewski, T., & Pasek, P. (2019). UWB-Based positioning system for supporting lightweight handheld Ground-Penetrating Radar. *2021 IEEE International Conference on Microwaves, Antennas, Communications and Electronic Systems (COMCAS)*, 1–4. https://doi.org/10.1109/comcas44984.2019.8958144

[13] Słowak, P., & Kaniewski, P. (2023). Homography augmented particle filter SLAM. *Metrology and Measurement Systems*. https://doi.org/10.24425/mms.2023.146420

[14] Laddach, K., Łangowski, R., & Zubowicz, T. (2022). Estimation of the angular position of a two–wheeled balancing robot using a real IMU with selected filters. *Bulletin of the Polish Academy of Sciences Technical Sciences*, 140518. https://doi.org/10.24425/bpasts.2022.140518

[15] Bar-Shalom, Y., Kirubarajan, T., & Li, X. R. (2001). *Estimation with applications to tracking and navigation: theory, algorithms, and software*. https://doi.org/10.1002/0471221279

[16] Kolat, M., Törő, O., & Bécsi, T. (2022). Performance evaluation of a maneuver classification algorithm using different motion models in a Multi-Model framework. *Sensors*, *22*(1), 347. https://doi.org/10.3390/s22010347

[17] Niewiara, Ł., Tarczewski, T., & Grzesiak, L. (2020). Application of extended Kalman filter for estimation of periodic disturbance and velocity ripple reduction in PMSM drive. *Bulletin of the Polish Academy of Sciences Technical Sciences*, 983–995. https://doi.org/10.24425/bpasts.2020.134649

[18] TDSR. (2020). *Data sheet/user guide: P440 UWB module*. https://tdsr-uwb.com/wp-content/uploads/2021/03/320-0317G-P440-Data-Sheet-User-Guide.pdf

Tomasz Kraszewski received his M.Sc. in 1999 and Ph.D. in 2023. He is currently a senior lecturer and researcher at the Institute of Radioelectronics, Faculty of Electronics at the Military University of Technology. His main research interests are the design and improvement nonlinear filtering in such applications as: localization, navigation and medical systems. He has authored more than 60 scientific papers.

Jarosław Panasiuk, PhD, Eng., is a graduate of the Military University of Technology in Warsaw. In 2004, he obtained a PhD in technical sciences with a specialization in mechanics. In 2007, he completed MBA studies at the Kozminski University in Warsaw. Currently, he works at the Faculty of Mechatronics and Aeronautics of the Military University of Technology and deals with issues related to robotization of production, modelling and design of robotics systems, as well as issues related to vision systems and building automation systems and neural networks. The scientific interests and research of Jarosław Panasiuk, PhD, Eng., focus on the subject of robot programming technology and robotization of production and vision systems, as well as innovative solutions in the field of building automation, artificial intelligence and weapon systems.

Metrol. Meas. Syst., Vol. 32 (2025), No. 3
DOI: 10.24425/mms.2025.154681

Paweł Leszek Słowak received his B.Sc. and M.Sc. degrees in mechatronics from the Military University of Technology in Warsaw, Poland in 2014 and 2015 respectively. He is currently an assistant lecturer and researcher at the Institute of Radioelectronics, Faculty of Electronics at the Military University of Technology. His research interests include simultaneous localization and mapping, multi-sensor fusion, navigation as well as radar target tracking.

Piotr Kaniewski received his M.Sc. in 1994, Ph.D. in 1998, and was habilitated in 2011. Currently he works as an Associate Professor at the Faculty of Electronics at the Military University of Technology. His research is focused on navigation systems for special purposes, such as supporting synthetic aperture radars and ground penetrating radars, on distributed estimation algorithms for UAV swarms, and navigation systems for GNSS denied environments. He has authored more than 200 scientific papers and 2 books.